Microscale Visualization of Microbial-Induced Calcium Carbonate Precipitation Processes

Yuze Wang, S.M.ASCE[1]; Kenichi Soga, Ph.D., M.ASCE[2];
Jason T. DeJong, Ph.D., M.ASCE[3]; and Alexandre J. Kabla, Ph.D.[4]

Abstract: Microbial-induced calcium carbonate ($CaCO_3$) precipitation (MICP) has been explored for its potential engineering applications such as soil stabilization, but current understanding of the fundamental MICP processes at the microscale is limited. In this study, real-time in situ microscale experiments were conducted using glass slides and microfluidic chips (synthetic porous media that simulate soil matrices to model the conditions similar to actual MICP treatments) to visualize the $CaCO_3$ precipitation process. The results of this study show that irregularly shaped $CaCO_3$ precipitates initially emerged on bacterial aggregates and subsequently dissolved with time as regularly shaped $CaCO_3$ crystals started growing; less stable and smaller $CaCO_3$ crystals may dissolve at the expense of growth of more stable and larger $CaCO_3$ crystals. The time-dependent phase transformation of $CaCO_3$ precipitates makes the size of the crystals formed during MICP highly dependent on the time interval between cementation solution injections during a staged-injection procedure. When the injection interval was 3–5 h, a larger number of crystals (200–1,000 per 10^6 μm^3) with smaller sizes (5–10 μm) was produced. When the injection interval was longer (23–25 h), the crystals were larger (10–80 μm) and fewer in number (5–20 per 10^6 μm^3). The direct observation of MICP processes in this study improves the understanding of MICP fundamentals and the effect of MICP processes on the properties of $CaCO_3$ crystals formed after MICP treatment. These observations will therefore be useful for designing future MICP treatment protocols that improve the properties and sustainability of MICP-treated samples. **DOI: 10.1061/(ASCE)GT.1943-5606.0002079.**

Introduction

Microbial-induced calcium carbonate precipitation (MICP) is a bio-geochemical process in which microbial activity alters the surrounding aqueous environment and induces calcium carbonate ($CaCO_3$) precipitation (Stocks-Fischer et al. 1999; DeJong et al. 2006). Due to its ease of control, high chemical conversion efficiency, and rapid operation process (Dhami et al. 2013), MICP occurring via a urea-hydrolysis pathway has been extensively studied for its potential subsurface applications such as soil stabilization (Whiffin et al. 2007; DeJong et al. 2006, 2010; van Paassen et al. 2010; Al Qabany and Soga 2013), erosion control (Jiang et al. 2017), and hydraulic control (Phillips et al. 2013). During the ureolysis-driven MICP process, bacteria with ureolytic activity express intracellular urea amidohydrolase, a urease enzyme that catalyzes the hydrolysis of urea [Eq. (1)]; the addition of calcium (Ca^{2+}) to this system induces the precipitation of calcium carbonate ($CaCO_3$) as the resulting CO_3^{2-} ions react with the supplied Ca^{2+} cations [Eq. (2)]

$$CO(NH_2)_2 + 2H_2O \xrightarrow{\text{Urease}} 2NH_4^+ + CO_3^{2-} \quad (1)$$

$$Ca^{2+} + CO_3^{2-} \rightarrow CaCO_3(s) \quad (2)$$

Research has shown that the $CaCO_3$ crystals can bond soil particles together, which strengthens the soil (DeJong et al. 2006, 2010) and can also fill the pores of the soil matrix, thus reducing soil permeability (Al Qabany and Soga 2013). This improvement in soil strength and permeability is not only dependent on the macroscale $CaCO_3$ content [mass of $CaCO_3$ precipitates divided by the total mass of $CaCO_3$ precipitates and soil particles, defined by Whiffin et al. (2007), van Paassen et al. (2010), and Al Qabany and Soga (2013)] but is also highly dependent on the microscale properties of $CaCO_3$ precipitates (DeJong et al. 2010; Al Qabany and Soga 2013; Lin et al. 2016; Wang et al. 2017). Previous MICP studies have shown a large variation in the microscale properties of $CaCO_3$ crystals, such as size and shape (van Paassen et al. 2010; Al Qabany and Soga 2013). However, the reasons for the formation of different sizes and shapes of $CaCO_3$ precipitates remain poorly understood.

$CaCO_3$ precipitates have a number of polymorphs, such as rhombohedral calcite (Kawano et al. 2002; Lian et al. 2006; Dhami et al. 2013), spherical vaterite (Kawano et al. 2002; Lian et al. 2006; van Paassen 2009; Dhami et al. 2013), aragonite, which normally crystallizes as clustered needles (Morse et al. 2007; Dhami et al. 2013) at high temperature [higher than 35°C (Ogino et al. 1987; Carteret et al. 2009)], and noncrystalline amorphous calcium carbonate (ACC) nanoparticles, which have a complex hybrid structure (Kawano et al. 2002; Bots et al. 2012; Dhami et al. 2013; Rodriguez-Blanco et al. 2011). Four images showing the

[1]Postdoctoral Researcher, Dept. of Engineering, Durham Univ., Durham DH1 3LE, UK; formerly, Ph.D. Research Student, Dept. of Engineering, Univ. of Cambridge, Cambridge, UK (corresponding author). ORCID: https://orcid.org/0000-0003-3085-5299. Email: yuze.wang@durham.ac.uk; yuzewang369@hotmail.com

[2]Chancellor's Professor, Dept. of Civil and Environmental Engineering, Univ. of California, Berkeley, CA 94720. Email: soga@berkeley.edu

[3]Professor, Dept. of Civil and Environmental Engineering, Univ. of California, Davis, CA 95616. Email: jdejong@ucdavis.edu

[4]Reader, Dept. of Engineering, Univ. of Cambridge, Cambridge CB2 1PZ, UK. ORCID: https://orcid.org/0000-0002-0280-3531. Email: ajk61@cam.ac.uk

Note. This manuscript was submitted on July 27, 2018; approved on February 4, 2019; published online on June 28, 2019. Discussion period open until November 28, 2019; separate discussions must be submitted for individual papers. This paper is part of the ***Journal of Geotechnical and Geoenvironmental Engineering***, © ASCE, ISSN 1090-0241.

$CaCO_3$ polymorphs reported in the literature are summarized in Fig. 1.

These $CaCO_3$ polymorphs not only vary in their morphology, but also vary in their stability and precipitation rate. Usually, the least-stable phase forms first and transforms into the next stable phase until finally, the most-stable phase forms [reviewed by Cöelfen and Antonietti (2008)]. The phase transformation during precipitation processes is consistent with Ostwald's step rule (Cöelfen and Antonietti 2008) and has been observed during $CaCO_3$ precipitation in previous studies. Wei et al. (2003) observed the transformation from vaterite to calcite. Kawano et al. (2002) and Rodriguez-Blanco et al. (2011) reported that ACC forms first and subsequently transforms to calcite via the intermediate formation of vaterite. With the phase transformation of $CaCO_3$ precipitates, the shape and size of the $CaCO_3$ precipitates change accordingly (Kawano et al. 2002; Bots et al. 2012). The phase transformations of $CaCO_3$ reported previously were based on the chemical precipitation of $CaCO_3$ induced by $CaCl_2$ and Na_2CO_3, rather than on the precipitation of $CaCO_3$ induced by bacteria. However, the similarities and differences between these two processes are as yet largely unknown. Furthermore, the shapes, sizes, and stabilities of $CaCO_3$ precipitates are very important factors that affect the engineering properties of MICP-treated soils (van Paassen 2009; DeJong et al. 2010; Al Qabany and Soga 2013; Lin et al. 2016; Wang et al. 2017). Therefore, a better understanding of (1) the phase transformation of $CaCO_3$ during MICP, and (2) the changes in shape and size of $CaCO_3$ precipitates with time will be helpful for designing MICP treatment protocols that improve the engineering properties of MICP-treated samples.

A widely held assumption of the $CaCO_3$ precipitation process during MICP is that bacterial cells serve as $CaCO_3$ nucleation sites and that once the nucleation sites form, the $CaCO_3$ crystals continue growing from them (Stocks-Fischer et al. 1999; Hammes and Verstraete 2002; DeJong et al. 2006; Dhami et al. 2013; Ganendra et al. 2014). This is assumed because bacterial cell walls are negatively charged and can adsorb Ca^{2+} (EI Mountassir et al. 2014). Therefore, once the bacterial cells hydrolyze the urea, the released CO_3^{2-} ions precipitate with the Ca^{2+} cations, which are attached to the bacterial cell walls, forming the $CaCO_3$ nucleation required for $CaCO_3$ crystal growth. However, this assumption has been questioned by the observation that $CaCO_3$ can precipitate in the absence of bacterial cells (Mitchell and Ferris 2006) and that some of the bacterial cells in the mixture of the bacterial suspension and the urea-$CaCl_2$ solution did not have $CaCO_3$ precipitates formed on them by 20 h after mixing (van Paassen 2009). In addition, $CaCl_2$ can cause the formation of bacterial aggregates which induce $CaCO_3$ precipitation (El Mountassir et al. 2014). However, because the microscope and digital camera used in these studies were not able to capture images at the bacterial size level, neither the effects of individual bacterial cells on the $CaCO_3$ nucleation and growth, nor the effects of bacterial aggregates on $CaCO_3$ precipitation are fully understood.

In this study, in situ microscale experiments were conducted with the following aims: (1) observe the evolution of the shape and size of the $CaCO_3$ precipitates during the MICP process, (2) understand the effects of bacterial cells/aggregates on $CaCO_3$ precipitation, and (3) vary the treatment procedure in an attempt to establish a correlation between the $CaCO_3$ precipitation process and the final size of $CaCO_3$ crystals. Microscale experiments were conducted using glass slides and microfluidic chips to simulate nonporous media and porous media where MICP processes occur. A high-resolution optical microscope capable of observing both bacterial cells and $CaCO_3$ precipitates in either glass slides or microfluidic chips was utilized. In the glass slide experiments, the MICP process after mixing the bacterial suspension with cementation solution was captured to explore the evolution of the shape and size of the $CaCO_3$ precipitates and the effects of bacterial cells/aggregates on $CaCO_3$ precipitation.

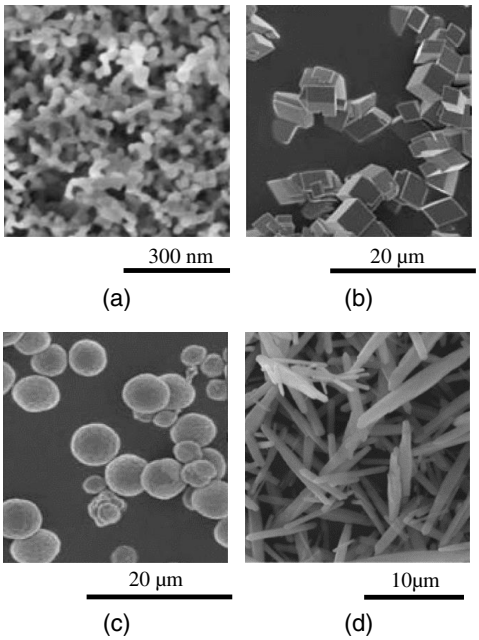

Fig. 1. Polymorphs of $CaCO_3$: (a) amorphous calcium carbonate (ACC); (b) calcite; (c) vaterite; and (d) aragonite. [Reprinted (a) with permission of RSC Pub, from *Nanoscale*, "The Kinetics and Mechanisms of Amorphous Calcium Carbonate (ACC) Crystallization to Calcite, Viavaterite," J. D. Rodriguez-Blanco, S. Shaw, and L. G. Benning, Vol. 3 (1), © 2011, permission conveyed through Copyright Clearance Center, Inc.; (b and c) with permission of RSC Pub, from *RSC Advances*, "CO2 Mineralization into Different Polymorphs of CaCO3 Using an Aqueous-CO2 System," D. H. Chu, M. Vinoba, M. Bhagiyalakshmi, H. Baek, S. C. Nam, Y. Yoon, S. H. Kim and S. K. Jeong, Vol. 3 (44), © 2013, permission conveyed through Copyright Clearance Center, Inc.; (d) with permission of RSC Pub, from *New Journal of Chemistry*, "Sonochemical Synthesis of Aragonite-Type Calcium Carbonate with Different Morphologies," G. T. Zhou, J. C. Yu, X. C. Wang, and L. Z. Zhang, Vol. 28 (8), © 2004, permission conveyed through Copyright Clearance Center, Inc.]

In the microfluidic chip experiments, microfluidic chips containing flow injection channels and synthetic porous media were used to observe the $CaCO_3$ precipitation process during staged-injection MICP procedures. These experiments involved a single injection of bacterial suspension followed by either 1, 2, or 12 injections of cementation solution with a time interval of either 3–5 or 23–25 h between injections. Three microfluidic chip experiments were conducted to explore (1) whether bacterial aggregation occurs during successive injections of bacterial suspension and cementation solution; (2) whether $CaCO_3$ precipitation occurs after the first and the second injections of cementation solution in the same way as observed in the glass slide experiment; and (3) whether different MICP treatment procedures produce $CaCO_3$ crystals with different sizes when the injection interval between two successive injections of cementation solution is varied. The practical implications of these findings are also discussed.

Materials and Methods

Bacterial Suspension

Sporosarcina pasteurii (*S. pasteurii*, strain DSM 33, purchased from DSMZ, Braunschweig, Germany) was used in the experiments described in this study. *S. pasteurii* is a naturally occurring strain of soil bacteria that has high ureolysis activity (Whiffin et al. 2007). The *S. pasteurii* bacterial suspension was prepared using a freeze-dried *S. pasteurii* stock, which was activated according to the manufacturer's guidelines (DSMZ, Braunschweig, Germany). After activation, glycerol stocks of the bacteria were prepared by adding 225 μL of 80% glycerol (autoclaved) to 1 mL of overnight liquid culture in cryogenic vials, after which the liquid culture was immediately frozen at −80°C. Once defrosted, cells from the glycerol stock were grown in American Type Culture Collection (ATCC) 1376 NH_4-YE agar medium (20 g/L yeast extract, 10 g/L ammonium sulfate, 20 g/L, agar and 0.13 M Tris base) for 48 h at 30°C. Subsequently, several colonies on the agar plate were picked and transferred to a NH_4-YE liquid medium containing the same components as ATCC 1376 NH_4-YE but without agar, and cultivated in a shaking incubator for 24 h at 30°C at a shaking rate of 200 rpm (rotations per minute) to obtain a bacterial suspension with an optical density measured at a wavelength of 600 nm (OD_{600}) of around 3.0. Because the type of enzyme produced by *S. pasteurii* is intracellular, there is no release of urease from the bacterial cells during cultivation. The bacterial suspension with lower OD_{600} was obtained by diluting this bacterial suspension using the NH_4-YE liquid medium.

Cementation Solution

The cementation solution for MICP treatment was created using calcium chloride dihydrate ($CaCl_2 \cdot 2H_2O$), urea ($CO(NH_2)_2$), and Thermo Scientific (Waltham, Massachusetts). Oxoid nutrient broth dissolved in deionized water. Two concentrations of calcium chloride were used: 0.25 and 1.0 M. The concentration of urea was 1.5 times higher than that of calcium chloride, and the concentration of nutrient broth was constant at 3 g/L. All chemicals used were of analytical reagent grade.

Glass Slide Experiment

Experiments on glass slides were conducted to examine the evolution of the shape and size of $CaCO_3$ precipitates in the mixture of bacterial suspension and cementation solution with time (Fig. 2). Glass slide samples were prepared by placing two successive 5-μL drops of bacterial suspension and cementation solution at the center of an optically transparent glass slide, after which an optically transparent cover slip was placed on top of the liquid specimen. Subsequently, the edges of the cover slips were sealed using nail varnish to avoid the drying of the liquid specimen on the glass slides (van Paassen 2009). The reported optical densities of bacterial suspension and concentration of cementation solution used during MICP treatment in the literature are in the range of 0.2–2.5 and 0.1–1.5 M, respectively (Al Qabany et al. 2012; Jiang et al. 2017; Cheng et al. 2017). The optical densities of bacterial suspension and the concentrations of cementation solution used in this study were within the range of the bacterial densities and concentrations of cementation solution reported in the literature and are given in Table 1.

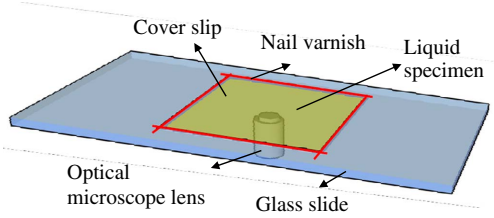

Fig. 2. Schematic of setup for glass slide experiments.

Table 1. Parameters of glass slide experiments

Experiment number	Sample ID	Content 1	Content 2
1	a	BS ($OD_{600} = 1$)	—
	b	BS ($OD_{600} = 1$)	CS (1 M)
	c	BS ($OD_{600} = 1$)	1 M $CaCl_2$
	d	BS ($OD_{600} = 1$)	1.5 M urea
	e	BS ($OD_{600} = 1$)	3 g/L nutrient broth
2	—	BS ($OD_{600} = 2.5$)	CS (1 M)

Note: BS = bacterial suspension; CS = cementation solution; and CS (1 M) contains 1 M $CaCl_2$, 1.5 M urea, and 3 g/L nutrient broth.

Test 1 was conducted to observe bacterial behavior after the bacterial suspension was mixed with cementation solution or with each of the individual components of the cementation solution. Test 2 was conducted to examine the evolution of the shape and size of $CaCO_3$ precipitates in the mixture of bacterial suspension and cementation solution with time. Time-series images of the sample in Test 2 were continuously captured at an imaging interval of 5 min over a time period of 12 h. The time 0 min or 0 h was the time when the first image of the sample was taken, which was about 2 min after mixing of bacterial suspension with the cementation solution.

Microfluidic Chip Experiments

A staged-injection procedure has been widely applied during MICP treatment for improving the strength and stability of soils (DeJong et al. 2006; Al Qabany and Soga 2013; Martinez et al. 2013; Montoya et al. 2013). During this injection procedure, a bacterial suspension was initially injected into a soil matrix and subsequently left to settle for several hours to enable bacteria to attach to the inner surface of the porous medium before the injection of the cementation solution. Normally, the injection of cementation solution was conducted in stages with an injection interval of 3–24 h between two subsequent injections. The glass slide experiment cannot simulate the flow of bacterial suspension and cementation solution through a porous soil matrix, which may affect the distribution of bacterial aggregates and individual bacterial cells, and which in turn may affect the properties of MICP-treated soils. In addition, in the glass slide experiment, bacterial suspension and cementation solution can only be mixed once, whereas in real MICP applications, the injection of cementation solution is normally repeated multiple times to increase the amount of $CaCO_3$ formed (van Paassen et al. 2010; Al Qabany et al. 2012). Therefore, after performing the glass slide experiments, microfluidic chip experiments were conducted to further explore the MICP process under conditions that more closely mimic MICP conditions that are present in real soils.

The schematic of the setup for the microfluidic chip experiments and the two-dimensional design of the microfluidic chip is shown in Fig. 3. The microfluidic chip was designed to create a two-dimensional model of the porous structure of a soil matrix based on a cross-sectional image of a solidified and sectioned three-dimensional Ottawa 30–50 sandy soil specimen and was fabricated using standard photolithography techniques. A cover slip made of polydimethylsiloxane (PDMS) that contained a matrix

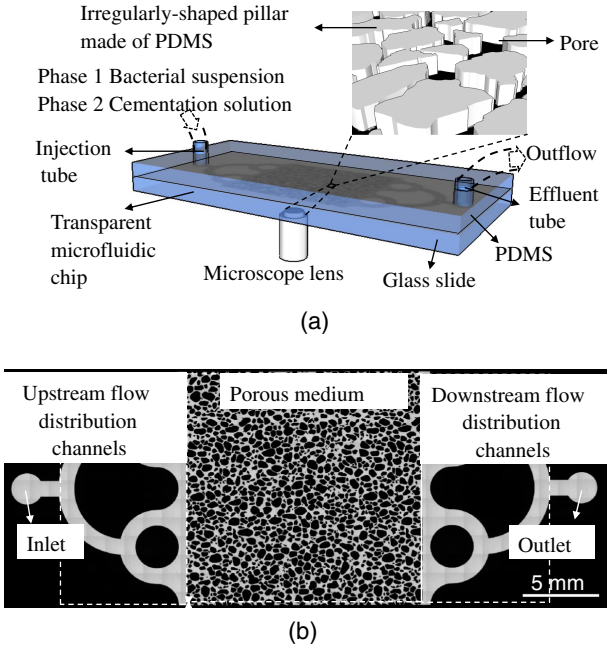

Fig. 3. (a) Schematic of setup for microfluidic chip experiments; and (b) two-dimensional design of the microfluidic chip.

of irregularly shaped pillars was bonded to a piece of glass slide by plasma treatment to create porous channels with pores to enable flow between the pillars [Fig. 3(a)]. Most of the distances between two adjacent pillars were shorter than 50 μm, roughly equivalent to the depth of the porous medium inside the microfluidic chip. Based on a two-dimensional design of the microfluidic chip, the calculated porosity of the porous medium inside the microfluidic chip was approximately 0.40 [Fig. 3(b)].

The microfluidic chip also contained an inlet and outlet to inject and let out the solution, respectively. Upstream and downstream flow distribution channels were used to homogeneously distribute the flow in and out of the porous medium [Fig. 3(b)]. A more detailed description of the design and fabrication process of the PDMS cover slip has been given by Wang et al. (2018). The experiments were conducted using both the microfluidic chip and a liquid injection system, which consisted of a syringe, syringe pump, and tubing. The injection system was used to inject the bacterial suspension and cementation solution into the microfluidic chip. The microfluidic chip is optically transparent, and the bacterial cells and the calcium carbonate inside the microfluidic chip can be observed under a high-resolution optical microscope.

Staged-injection MICP procedures were applied in three microfluidic chip experiments. The parameters of bacterial suspension and bacterial injection were the same in these three experiments. The OD_{600} of the bacterial suspension measured prior to the bacterial injection was 1.0. The injection flow rate of bacterial suspension was 0.5 mL/h, and the calculated Darcy velocity is 4.6×10^{-4} m/s at this injection flow rate. The volume of the bacterial suspension injected (11.25 μL) was 1.25 times higher than the pore volume of the microfluidic chip (9 μL). After the injection of bacterial suspension, the bacteria were given 24 h to attach to the inner surface of the porous medium prior to the injection of cementation solution. The cementation solution used in all of the three microfluidic chip experiments was constant and contained 0.25 M $CaCl_2$, 0.375 M urea, and 3 g/L nutrient broth. In addition, the volume of the cementation solution injected during each injection was also constant, which was 1.25 times higher than the pore volume of the microfluidic chip. However, the other parameters associated with the cementation solution injection were varied in the three experiments and are summarized in Table 2.

In the first experiment, two injection flow rates of cementation solution were applied, which were 0.05 and 0.5 mL/h, corresponding to Darcy velocities of 4.6×10^{-5} m/s and 4.6×10^{-4} m/s, respectively. This experiment was conducted to explore the behavior of bacteria after injecting cementation solution at different flow rates. In the second experiment, two injections of cementation solution were applied to explore whether the $CaCO_3$ precipitation occurs after the first and the second injections of the cementation solution in the same way as observed in the glass slide experiment. The third experiment was conducted to explore whether different MICP treatment procedures produce $CaCO_3$ crystals with different sizes when the injection interval between two successive injections of cementation solution is varied. In this experiment, 12 injections of cementation solution were applied, with intervals of either 3–5 h or 23–25 h between successive injections. For each protocol, a newly fabricated microfluidic chip was used.

Microscale Visualization and Image Quantification

Images of samples were taken using an optical microscope (Zeiss Axio Observer Z1, Oberkochen, Germany) to visualize the bacterial cells and $CaCO_3$ precipitates. The microscope was equipped with a black and white camera (Hamamatsu C11440-22CU, Hamamatsu, Japan) connected to a computer. Images were taken using phase field illumination and 10× inverted objective with an image resolution of 0.65 μm/pixel. The image of $CaCO_3$ precipitates is brighter than both bacterial cells and the solution under the optical microscope in phase field. To quantify the size of individual crystals, the diameters or lengths of the crystals in the two-dimensional (2D) images were measured using ZEN 2 software. The number of crystals present in selected areas of the images were also counted to quantify the number of crystals formed in a unit area.

Results of Microscope Slide Experiments and Discussion

Bacterial Aggregation

In the first glass slide experiment, microscope images of several samples containing the bacterial suspension or mixtures of bacterial

Table 2. Parameters of cementation solution injection in the microfluidic chip experiments

Experiment number	Protocol number	Flow rate (mL/h)	Injection number	Injection frequency per day	Injection intervals (h)	Total treatment duration (days)
1	1_1	0.05	1	—	—	—
	1_2	0.5	1	—	—	—
2	2	0.05	2	Once	24	2
3	3_1	0.05	12	2–4 times	3–5	4
	3_2	0.05	12	Once	23–25	12

J. Geotech. Geoenviron. Eng., 2019, 145(9): 04019045

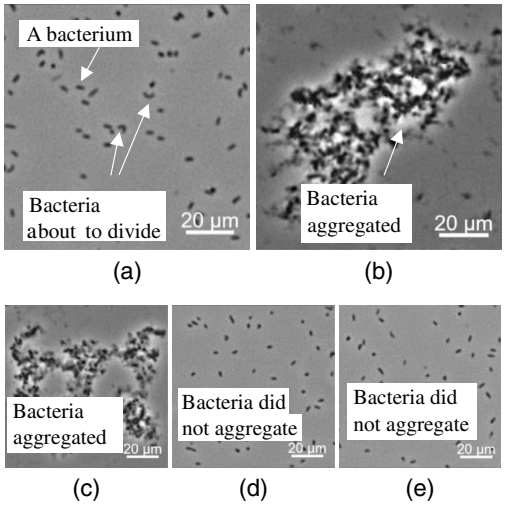

Fig. 4. Optical microscope images: (a) bacterial suspension ($OD_{600} = 1.0$) in which bacteria did not aggregate; (b) mixture of equal volumes of bacterial suspension ($OD_{600} = 1.0$) and cementation solution (1.0 M $CaCl_2$, 1.5 M urea, and 3 g/L nutrient broth) in which bacteria aggregated; (c) mixture of equal volumes of bacterial suspension ($OD_{600} = 1.0$) and $CaCl_2$ solution (1.0 M) in which bacteria aggregated; (d) mixture of equal volumes of bacterial suspension ($OD_{600} = 1.0$) and urea solution (1.5 M) in which bacteria did not aggregate; and (e) mixture of equal volumes of bacterial suspension ($OD_{600} = 1.0$) and nutrient broth (3 g/L) in which bacteria did not aggregate.

suspension with each of the main components of the cementation solution were captured and compared with images taken after mixing the bacterial suspension with the cementation solution (Fig. 4). Fig. 4(a) shows a sample containing *S. pasteurii* suspension. The *S. pasteurii* cells were about 3 μm in length and were rod shaped, which is consistent with the size and shape of *S. pasteurii* cells observed by scanning electron microscopy (Bang et al. 2001; Keykha et al. 2015). The *S. pasteurii* cells did not aggregate in the bacterial suspension [Fig. 4(a)]. This might be due to the repulsive forces between bacterial cells. In the presence of cementation solution, the bacteria aggregated [Fig. 4(a) compared with Fig. 4(b)], which is consistent with the images of van Paassen (2009). In addition, *S. pasteurii* cells aggregated in the presence of $CaCl_2$ [Fig. 4(c)], but not in the presence of urea or nutrient broth [Figs. 4(d and e)]. This suggests that the $CaCl_2$ contained in the cementation solution is the component that induced bacterial aggregation, which is consistent with previous findings reported in the literature (El Mountassir et al. 2014).

Evolution of $CaCO_3$ *Precipitate Size and Shape during MICP*

Time-series images of the mixture of bacterial suspension and cementation solution that were taken over 12 h are shown in Fig. 5. Bacterial aggregation and $CaCO_3$ precipitation started immediately after the mixing [Fig. 5(a)], which is consistent with the observation made by van Paassen (2009). The shapes of both bacterial aggregates (BAs) and $CaCO_3$ precipitates at the initial stage were irregular [Fig. 5(a)]. By 30 min after mixing, more irregularly shaped

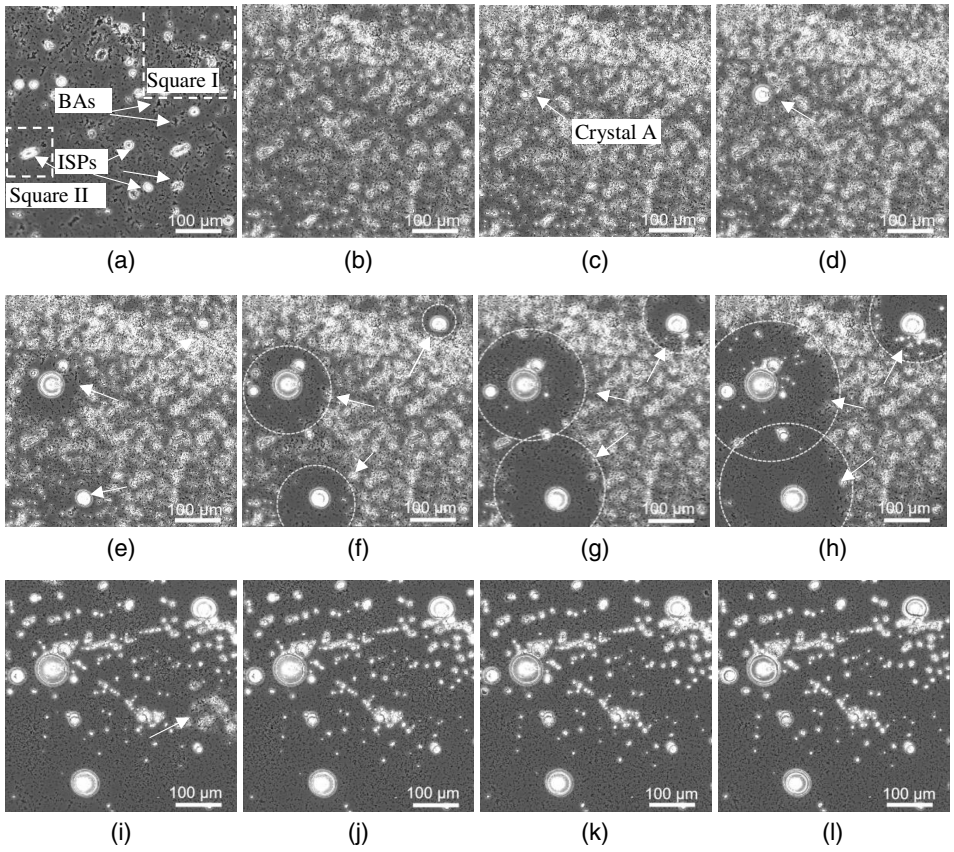

Fig. 5. Time-lapse microscope images of microscope glass slides containing the mixture of bacterial suspension and cementation solution: (a) 0 min; (b) 30 min; (c) 50 min; (d) 1 h; (e) 1 h 10 min; (f) 1 h 15 min; (g) 1 h 20 min; (h) 1 h 25 min; (i) 1 h 45 min; (j) 2 h; (k) 6 h; and (l) 12 h.

J. Geotech. Geoenviron. Eng., 2019, 145(9): 04019045

$CaCO_3$ precipitates (ISPs) formed [Fig. 5(b)], shown by more areas in the image becoming brighter at 30 min compared with 0 min. The irregularly shaped $CaCO_3$ precipitates continued growing until 50 min, when one spherical $CaCO_3$ crystal (Crystal A) appeared [circular in the 2D image, Fig. 5(c)]. After that, the irregularly shaped $CaCO_3$ precipitates surrounding Crystal A started dissolving. The area containing dissolving irregularly shaped $CaCO_3$ became larger with the growth of Crystal A [Fig. 5(e) compared with Fig. 5(d)]. In the meantime, several new crystals formed [Fig. 5(e) compared with Fig. 5(d)].

The zones where the irregularly shaped $CaCO_3$ precipitates dissolved were not only increasing in size with the growth of the crystals, but also had a circular shape [Figs. 5(f–h)]. By 1 h and 45 min, some undissolved irregularly shaped $CaCO_3$ precipitates [Fig. 5(i)] remained, but by 2 h, all dissolved [Fig. 5(j)]. Between 2 and 12 h, all of the existing $CaCO_3$ precipitates were regularly shaped crystals [Figs. 5(i–l)]. Therefore, in general, the overall MICP process between 0 and 12 h after the mixing of bacterial suspension and cementation solution can be divided into the following three main stages: (1) bacterial aggregation, which occurs immediately after the mixing of bacterial suspension with cementation solution; (2) growth of irregularly shaped $CaCO_3$ precipitates (0–1 h); and (3) dissolution of irregularly shaped $CaCO_3$ precipitates (1–2 h) at the expense of the growth and formation of regularly shaped $CaCO_3$ crystals (1–12 h).

The irregularly shaped $CaCO_3$ precipitates formed during the initial stage of $CaCO_3$ precipitation were not stable and dissolved easily with the precipitation of the regularly shaped $CaCO_3$ crystals, which is consistent with the observations made by Kawano et al. (2002). According to Ostwald's step rule, amorphous $CaCO_3$ (ACC), which is the most unstable form of $CaCO_3$, is the first to precipitate during $CaCl_2$-induced and Na_2CO_3-induced chemical precipitation of $CaCO_3$. This is because ACC has the highest solubility among all the $CaCO_3$ precipitates, and because the concentrations of Ca^{2+} and CO_3^{2-} in the mixed solution drop to the solubility for ACC during its precipitation while still being high enough for more stable $CaCO_3$ crystals such as vaterite and calcite to nucleate and grow (Kawano et al. 2002). In the present study, the $CaCO_3$ precipitates that formed first were irregularly shaped and had higher solubility compared with the crystal form of $CaCO_3$ precipitates, which is consistent with the parameters of amorphous-phase $CaCO_3$ (Kawano et al. 2002; Bots et al. 2012; Dhami et al. 2013; Rodriguez-Blanco et al. 2011). In addition, the irregularly shaped $CaCO_3$ precipitates dissolved around the crystals that formed; the shapes of the zones where the irregularly shaped $CaCO_3$ precipitates dissolved were circular, and these areas increased with the growth of the $CaCO_3$ crystals. These observations also suggest that the crystals grew at the expense of the dissolution of the irregularly shaped $CaCO_3$ precipitates (Kawano et al. 2002). The $CaCO_3$ precipitation process observed in this study is consistent with the process observed by Kawano et al. (2002), in which unstable $CaCO_3$ precipitated first and then dissolved when more stable crystals precipitated. However, the precipitation of $CaCO_3$ in the study by Kawano et al. (2002) was caused by the chemical reaction between $CaCl_2$ and Na_2CO_3, rather than by biochemical reactions due to bacterial activity.

Because the magnification level in the images shown in Fig. 5 is not high enough to observe the details of bacterial cells and $CaCO_3$ crystals, images taken at higher magnification levels (Squares I and II in Fig. 5) are presented and discussed in the next two subsections to observe more details regarding the precipitation and dissolution of irregularly shaped $CaCO_3$ precipitates and the evolution of $CaCO_3$ crystals.

Precipitation and Dissolution of Irregularly Shaped $CaCO_3$ Crystals

Magnified images of Square I in Fig. 5(a) at selected time points (0, 20, and 50 min) are shown in Figs. 6(a–c) to observe whether individual bacterial cells or bacterial aggregates have an effect on the nucleation and growth of $CaCO_3$ precipitates. To observe the images in more detail, magnified images of the square in Figs. 6(a–c) are shown in Figs. 6(d–f).

A large amount of the bacterial cells aggregated, and irregularly shaped $CaCO_3$ precipitates started forming immediately after the start of the imaging process [indicated by the arrow in Fig. 6(a)]. The irregularly shaped $CaCO_3$ precipitates formed mostly on bacterial aggregates [indicated by the arrow in Figs. 6(b and c)] and occasionally also formed on individual bacterial cells [indicated by the arrow in Fig. 6(f)]. The $CaCO_3$ precipitates continued to grow from 0 to 50 min, as shown by the image pixels becoming brighter [Fig. 6(b) compared with Fig. 6(a), or Fig. 6(c) compared with Fig. 6(b)]. The time at which the precipitates started forming varied, with some of these forming at 0 min, whereas others formed after 20 min.

The images in Fig. 6 suggest that bacterial aggregation affects the formation of irregularly shaped $CaCO_3$ precipitates. Based on Eqs. (1) and (2), bacteria hydrolyze urea and produce CO_3^{2-} ions, which react with Ca^{2+} to form $CaCO_3$. Assuming that the ureolysis capacity of each bacterial cell is the same, bacterial aggregates containing a large number of bacteria are more effective at hydrolyzing urea compared with individual bacterial cells. Therefore, the concentration of CO_3^{2-} surrounding the bacterial aggregates increases more quickly. In addition, the bacterial aggregates contained a large amount of Ca^{2+} surrounding the bacterial cells, thus causing $CaCO_3$ to precipitate on bacterial aggregates more quickly. As the local concentration of urea surrounding the bacterial aggregates decreases, more urea diffuses to them, thus resulting in the continued precipitation of $CaCO_3$ on the bacterial aggregates.

This observation suggests that bacterial aggregates formed during the initial stage of $CaCO_3$ precipitation, and that they had an effect on $CaCO_3$ precipitation where the precipitates grew on top of bacterial aggregates. In addition, individual bacterial cells affected

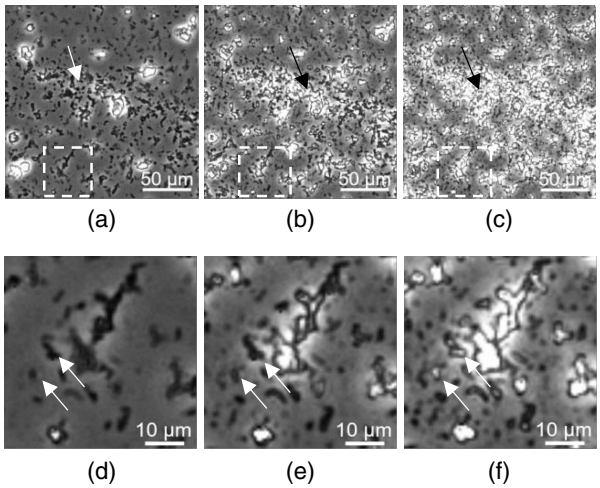

Fig. 6. Microscope images showing the precipitation of irregularly shaped $CaCO_3$ crystals and the fixation of bacterial cells during the precipitation process: (a) 0 min; (b) 20 min; (c) 50 min; (d) 0 min; (e) 20 min; and (f) 50 min. Magnified images of squares in plots (a)–(c) are shown in plots (d)–(f), respectively:

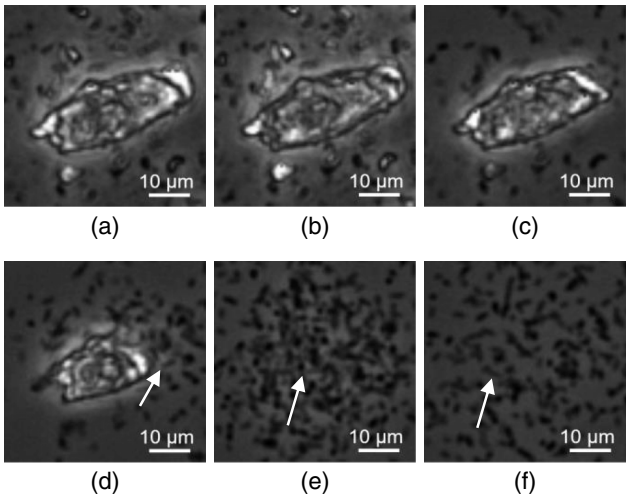

Fig. 7. Dissolution of an irregularly shaped $CaCO_3$ precipitate and the movement of bacterial cells after the dissolution of the $CaCO_3$ precipitate: (a) 30 min; (b) 1 h; (c) 1 h 20 min; (d) 1 h 15 min; (e) 1 h 30 min; and (f) 2 h.

the precipitation of irregularly shaped $CaCO_3$ precipitates, but the effect of individual bacterial cells was less when compared with the effect of bacterial aggregates.

To observe the dissolution of irregularly shaped $CaCO_3$ precipitates in more detail, magnified images of Square II [Fig. 5(a)] at selected time points (between 30 min and 2 h) are shown in Fig. 7. With the dissolution of the irregularly shaped $CaCO_3$ precipitate, the bacterial cells become free to move [indicated by the arrows in Figs. 7(d, e, and f)]. *S. pasteurii* belongs to the genus Bacillus and the mobility of *S. pasteurii* is consistent with that of Bacillus bacteria (Yoon et al. 2001). These observations suggest that bacterial aggregation and the formation of irregularly shaped $CaCO_3$ precipitates encapsulate bacterial cells. By contrast, because the irregularly shaped $CaCO_3$ precipitates were not stable, the dissolution of the irregularly shaped $CaCO_3$ resulted in the bacterial cells becoming free to move again.

Dissolution of Irregularly Shaped $CaCO_3$ *and Reprecipitation of* $CaCO_3$ *Crystals*

To observe the precipitation process and stabilities of $CaCO_3$ crystals in more detail, including the evolution of their shape and size,

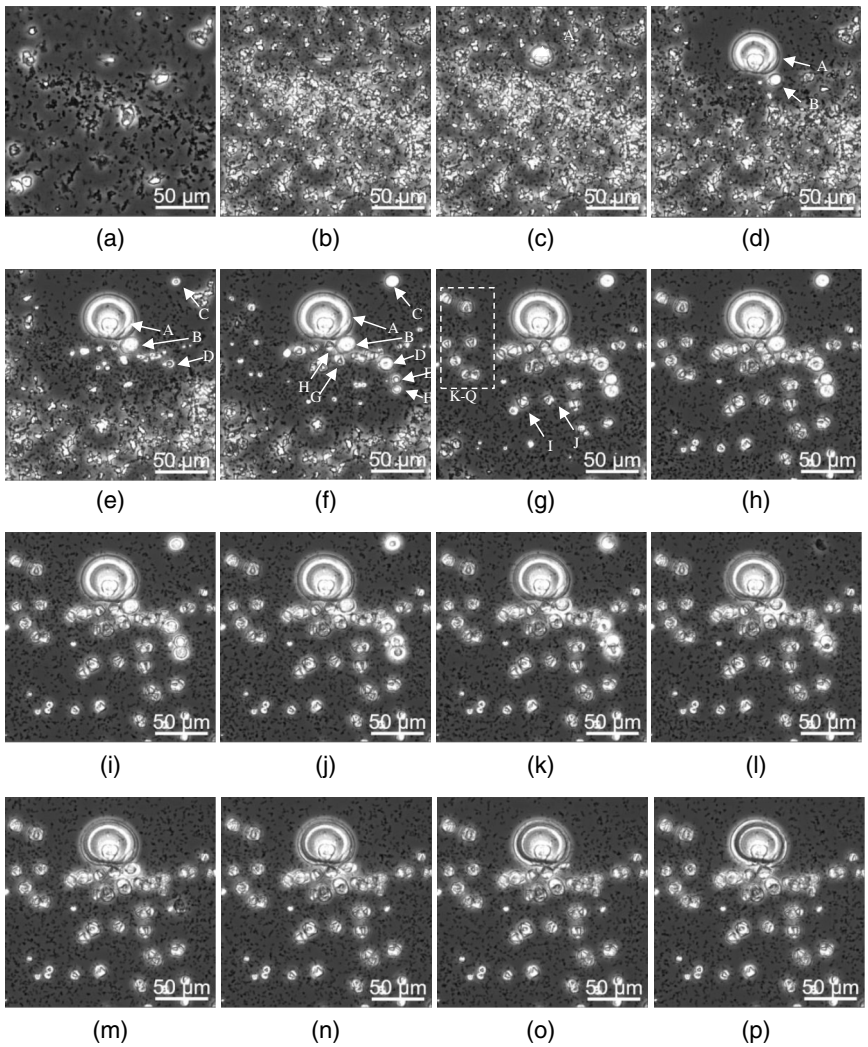

Fig. 8. Microscope images showing the dissolution of spherical $CaCO_3$ crystals while rhombohedral $CaCO_3$ crystals continued to be stable: (a) 0 h; (b) 1 h; (c) 1 h 10 min; (d) 1 h 20 min; (e) 1 h 25 min; (f) 1 h 30 min; (g) 1 h 40 min; (h) 2 h; (i) 3 h; (j) 4 h; (k) 5 h; (l) 6 h; (m) 7 h; (n) 8 h; (o) 10 h; and (p) 12 h.

J. Geotech. Geoenviron. Eng., 2019, 145(9): 04019045

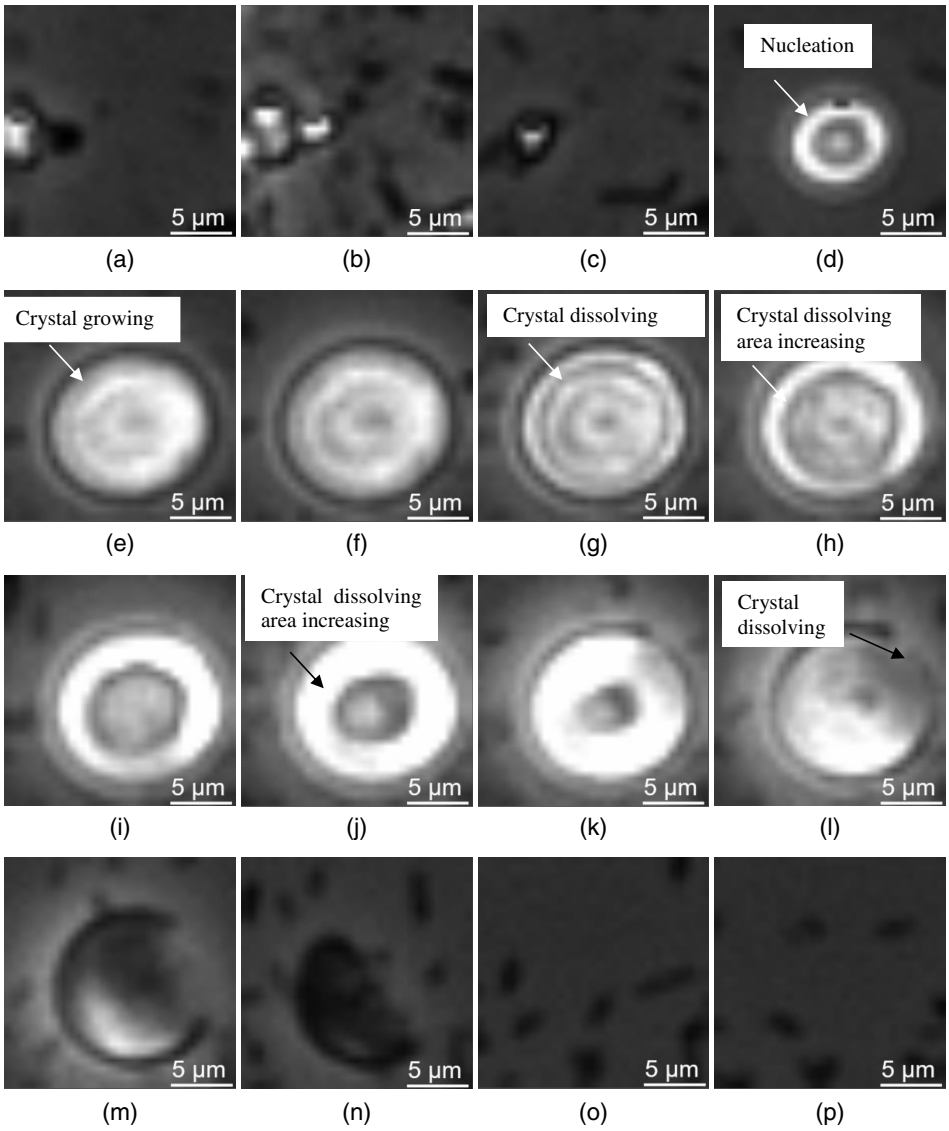

Fig. 9. Microscope images showing the growth and dissolution of a spherical $CaCO_3$ crystal: (a) 0 h; (b) 1 h; (c) 1 h 20 min; (d) 1 h 25 min; (e) 1 h 30 min; (f) 2 h; (g) 2 h 30 min; (h) 3 h; (i) 3 h 30 min; (j) 4 h; (k) 4 h 30 min; (l) 5 h; (m) 5 h 30 min; (n) 6 h; (o) 7 h; and (p) 12 h.

magnified images of Square I in Fig. 5(a) at selected time points are shown in Fig. 8. As can be seen from this figure, $CaCO_3$ crystals grew with the dissolution of the irregularly shaped $CaCO_3$ precipitates. Most crystals were spherical, such as Crystals A–F, or rhombohedral, such as Crystals G–Q. The spherical and rhombohedral shapes of $CaCO_3$ crystals are consistent with the shapes of vaterite and calcite, respectively (Kawano et al. 2002; Chu et al. 2013). Spherical crystals were not stable and dissolved later on. For example, Crystal B dissolved by 12 h and Crystals C–F dissolved by 7 h. Rhombohedral crystals such as Crystals G–Q were stable and did not dissolve after being formed.

To observe the formation of spherical and rhombohedral $CaCO_3$ crystals in more detail, such as changes in their shape and size with time, magnified images of Crystals C and I, which are shown in Fig. 8, were selected to be representative, and their shapes at selected time points are shown in Figs. 9 and 10, respectively.

The spherical Crystal C started to form by 1 h 25 min [Fig. 9(d)], and then grew until 2 h [Fig. 9(f)], after which it started to dissolve and became fully dissolved by 7 h [Fig. 9(o)]. Therefore, spherical Crystal C is relatively unstable. This dissolution of spherical crystals is consistent with the dissolution of vaterite according to Ostwald's step rule, as well as with the Scanning electron microscope (SEM) images showing the dissolved vaterite (van Paassen 2009) taken 1 week after MICP treatment. In contrast, the rhombohedral crystal (Crystal I) was stable once it formed [Figs. 10(d–l)].

These results are consistent with several studies where the percentage of rhombohedral $CaCO_3$ crystals relative to all crystals increased at later stages during the precipitation process (Wei et al. 2003; Rodriguez-Blanco et al. 2011). However, the results presented in this study are the first direct observation of the process of dissolution of spherical $CaCO_3$ crystals at an expense of further growth of rhombohedral crystals.

Results of Microfluidic Chip Experiments and Discussion

The $CaCO_3$ precipitation process shown in the glass slide experiment represents the process occurring after the bacterial suspension was mixed with the cementation solution. However, this does

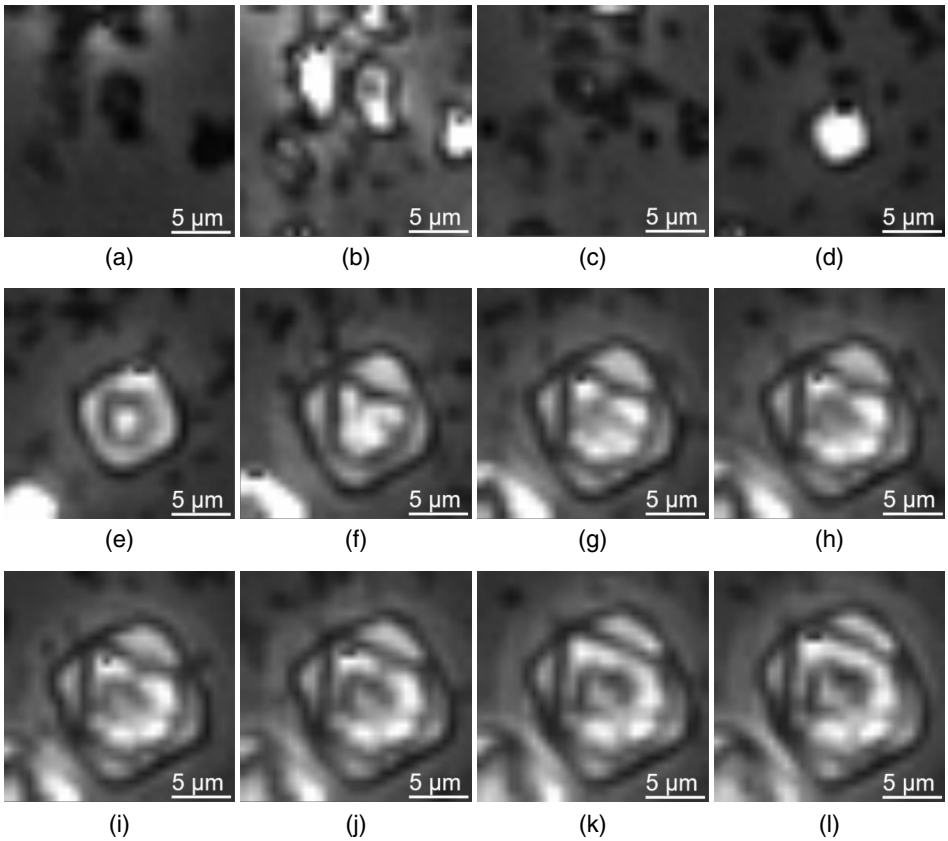

Fig. 10. Microscope images showing growth of a rhombohedral $CaCO_3$ crystal: (a) 0 h; (b) 1 h; (c) 1 h 20 min; (d) 1 h 30 min; (e) 1 h 35 min; (f) 1 h 40 min; (g) 1 h 45 min; (h) 1 h 50 min; (i) 2 h; (j) 4 h; (k) 8 h; and (l) 12 h.

not fully represent the actual MICP process in which the bacterial suspension and cementation solution are successively injected into a soil matrix (DeJong et al. 2006; Al Qabany and Soga 2013; Martinez et al. 2013; Montoya et al. 2013). The objectives of the microfluidic experiments were to (1) observe bacterial aggregation during sequential injections of bacterial suspension and cementation solution; (2) observe $CaCO_3$ crystal formation after each of the cementation solution injections; (3) examine the movement of $CaCO_3$ precipitates with the flow; and (4) investigate various MICP treatment procedures, during which the time interval between successive injections of cementation solution was varied to establish a correlation between the $CaCO_3$ precipitation processes and the final size of $CaCO_3$ crystals.

Bacterial Behavior after Staged Injections of Bacteria and Cementation Solution

The first microfluidic experiment was conducted to observe bacterial aggregation during a staged-injection MICP process. Two protocols (Protocols 1_1 and 1_2) were applied, and the experimental parameters are summarized in Table 2. The difference between these two protocols is the injection flow rate of cementation solution, which were 0.05 and 0.5 mL/h, corresponding to Darcy velocities of 4.6×10^{-5} m/s and 4.6×10^{-4} m/s, respectively. These values are within the range of values reported in the literature (Al Qabany and Soga 2013; Martinez et al. 2013; Montoya et al. 2013).

Bacterial cells continued to grow even after being injected, as shown by the difference in the number of bacteria present between Figs. 11(a and b). A large proportion of bacterial cells were flushed out after the injection of cementation solution [Figs. 11(c and d) compared with Fig. 11(b)]. In an open pore, fewer bacterial cells remained after the injection of cementation solution when the injection flow rate of cementation solution was 10 times higher [Fig. 11(d) compared with Fig. 12(c)]. On the other hand, bacterial aggregation and precipitation of irregularly shaped $CaCO_3$ occurred after the injection of cementation solution either in narrow pore throats or on vertical surfaces within the microfluidic chips at both flow rates [Figs. 11(e and f)]. The bacteria fixed by the irregularly shaped $CaCO_3$ crystals were no longer aggregated by 24 h [Figs. 11(g and h)].

The results of this experiment suggest that the bacterial cells did not aggregate after injection or after settling, but that some of them aggregated after the injection of cementation solution, even though this aggregation was less extensive compared with the bacterial cells that aggregated in the mixture of bacterial suspension and cementation solution in the glass slide samples. This is because bacterial cells were relatively well mixed with the Ca^{2+} ions of the cementation solution in a glass slide sample, which resulted in relatively large quantities of bacterial aggregates. However, in the staged-injection microfluidic chip experiment, the bacterial cells were only aggregated by Ca^{2+} at the interface between the bacterial suspension and cementation solution, where bacterial cells dispersed into the cementation solution and Ca^{2+} diffused into the bacterial suspension. The injection of the cementation solution pushed the interface between these two liquids forward toward the outlet of the microfluidic chip, with bacterial aggregates becoming filtered or adsorbed by the porous medium during the injection of cementation solution. The flow rate affects bacterial detachment at open pores, where fewer bacteria remained after the injection of

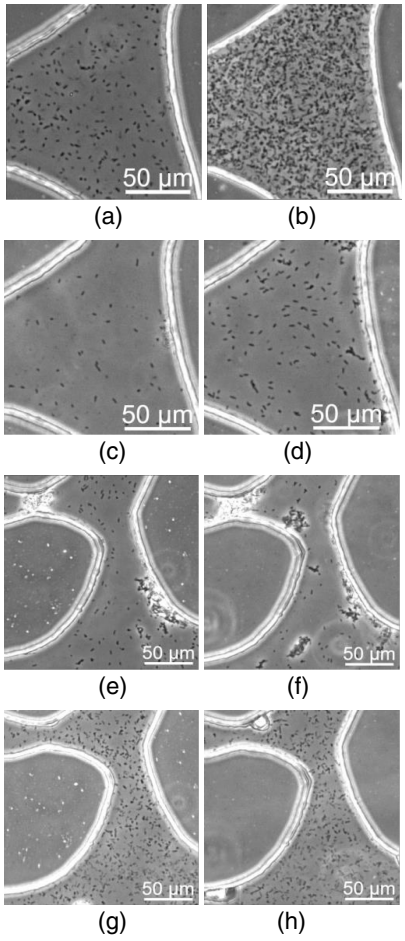

Fig. 11. Microscope images of bacteria inside the central pores of the microfluidic chip at different stages of the MICP process: (a) after the injection of bacterial suspension; (b) after bacterial settling; (c) after the injection of cementation solution injection at 0.5 mL/h, open pore; (d) after the injection of cementation solution injection at 0.05 mL/h, open pore; (e) after the injection of cementation solution injection at 0.5 mL/h, narrow pore; (f) after the injection of cementation solution injection at 0.05 mL/h, narrow pore; (g) 24 h after cementation solution injection at 0.5 mL/h; and (h) 24 h after cementation solution injection at 0.05 mL/h.

cementation solution when the flow rate was higher (0.5 mL/h, with a calculated Darcy velocity of 4.6×10^{-4} m/s) compared with a flow rate of 0.05 mL/h. However, because bacterial aggregates became trapped within the narrow pores after the injection of cementation solution at both flow rates (0.5 and 0.05 mL/h), the number of bacteria remaining in the porous medium after the injection of cementation solution was similar at both flow rates.

Crystal Formation after Injection of Cementation Solution

The second microfluidic chip experiment was conducted to examine the $CaCO_3$ precipitation process during an MICP procedure involving a single injection of bacterial suspension followed by two subsequent injections of cementation solution. Fig. 12 shows the time-series images of five pores in the microfluidic chip taken directly after the first injection of cementation solution, and at 1, 3, and 24 h after the injection. Consistent with the results obtained from the glass slide experiment, bacterial cells aggregated, although to a smaller extent compared with that in the glass slide experiment (Fig. 12 images of Pores I, II, III, and V at 0 h). Furthermore, irregularly shaped $CaCO_3$ precipitates (ISPs) were formed (Fig. 12 images of Pores I, II, III, and V at 0 h). The irregularly shaped $CaCO_3$ precipitates continued to grow from 0 to 1 h (Fig. 12 images of Pores I, II, III, and V takes at 1 h compared with the 0-h images) and then dissolved (Fig. 12 images of Pores I and II at 3 h and Pores III and V taken at 24 h compared with 0-h photos). With the dissolution of the irregularly shaped $CaCO_3$ precipitates, the bacterial cells that were enclosed became dispersed (Fig. 12 images of Pores I and II at 3 h). $CaCO_3$ crystals appeared with the dissolution of the irregularly shaped $CaCO_3$ precipitates (such as the Pore V 3-h photo compared with the 1-h photo). Finally, the spherical crystals dissolved but the other crystals remained (Pore IV 24-h image).

In Fig. 13, images of Pore V at 0, 1, 3, and 24 h after the completion of the second injection of cementation solution are presented. The two crystals that formed after the first injection of cementation solution were still at the same place inside the pore after the second injection of the cementation solution. This suggests that the crystals were stable inside the porous medium and could not be flushed out at a flow rate of 0.05 mL/h. At 3 h, small crystals formed (bright dots in Fig. 13). However, by 24 h, the small crystals dissolved. The big crystals in these two pores continued to grow during the first 24 h, after which only the big crystals and several newly formed crystals remained.

Effect of Injection Interval on the Size of $CaCO_3$ Crystals

The results from the second microfluidic chip experiment suggest that the unstable $CaCO_3$ crystals dissolved at the expense of the growth of more stable crystals after the first and second injection of cementation solution. The dissolution of the unstable crystals occurred between 3 and 24 h after each of the injections, suggesting that the final crystal size would be different if the injection interval was to be shorter than 24 h. The third microfluidic chip experiment was conducted by varying the time interval between subsequent injections of cementation solution. The experimental parameters are given in Table 2. The first protocol (Protocol 3_1) had a short injection interval (3–5 h interval and injected 2–4 times per day), whereas the second protocol (Protocol 3_2) had a longer interval of 23–25 h (injected once per day). Images taken at the middle of the two microfluidic chips 1 day after the final (12th) injection of cementation solution are shown in Fig. 14(a). Magnified images of the two squares in these two images depicted in Fig. 14(a) are shown in Fig. 14(b) to show the crystals in more detail.

Figs. 14(a and c) show the crystals formed during the short injection interval protocol (Protocol 3_1). The sizes of spherical crystals were small (5–10 μm), but the number of crystals was high (200–1,000 per 10^6 μm^3) [Figs. 14(a and c)]. The crystals coated the inner surface of the microfluidic chip. Small crystals remained inside the pores because a 3–5 h retention time was not long enough for every small crystal to dissolve.

Figs. 14(b and d) show the crystals formed during the long-injection-interval protocol (Protocol 3_2). The sizes of $CaCO_3$ crystals are larger (10–80 μm) than those in Protocol 3_1. The number of crystals inside the pores is small (5–20 per 10^6 μm^3), which is about 1/40 the number of crystals observed in Protocol 3_1. A 23–25-h retention time resulted in smaller spherical crystals being dissolved, and the calcium cations produced by this dissolution process formed larger crystals.

Al Qabany et al. (2012) concluded that the size of $CaCO_3$ crystals formed was smaller when soil samples were treated more

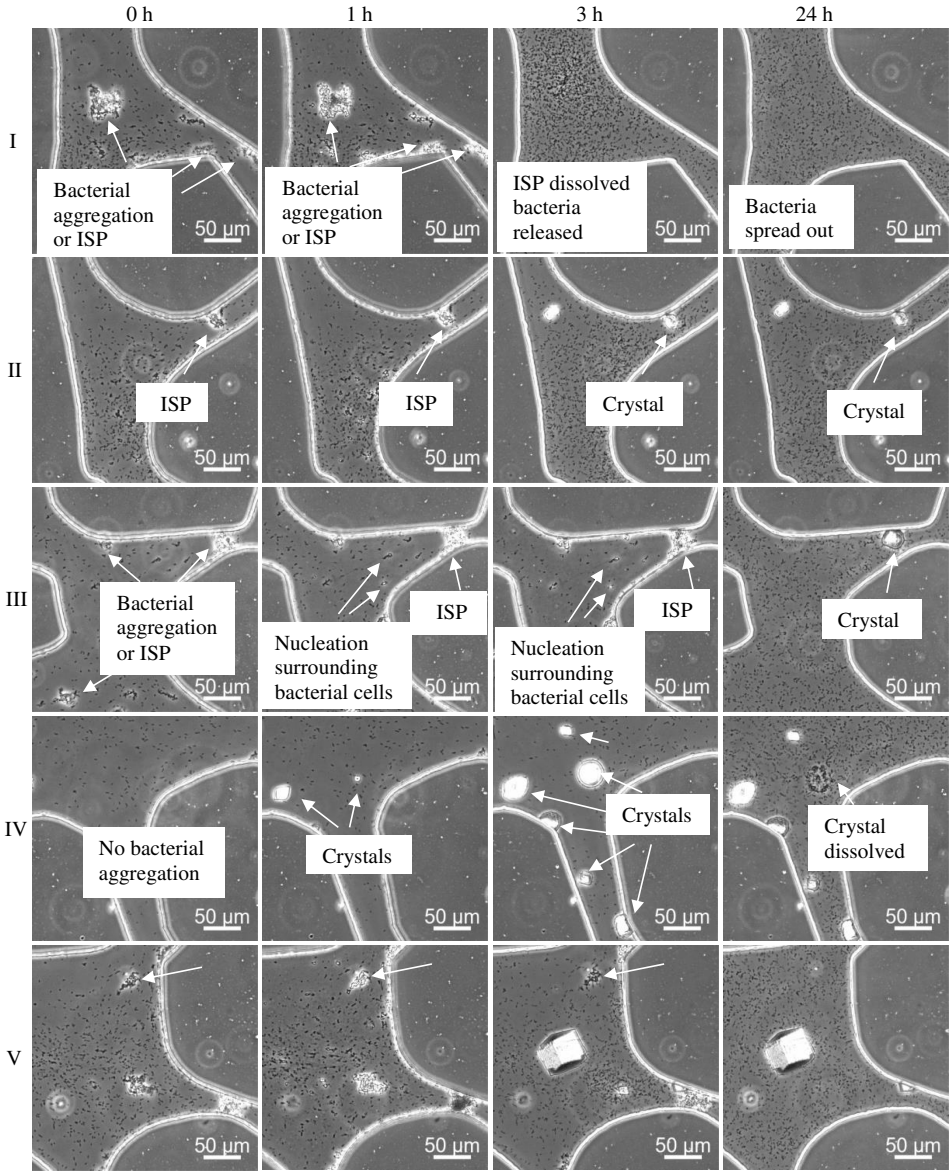

Fig. 12. Microscope images of five pores in the microfluidic chip (Protocol 2) at 0, 1, 3, and 24 h after first injection of cementation solution.

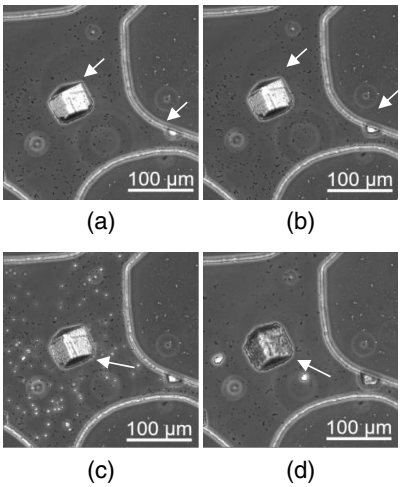

Fig. 13. Microscope images of Pore V in the microfluidic chip (Protocol 2) after the second injection of cementation solution: (a) 0 h; (b) 1 h; (c) 3 h; and (d) 24 h.

frequently with a lower concentration of cementation solution compared with soil samples that were treated less frequently with a higher concentration of cementation solution. In light of this finding, the present study's results suggest that when the concentration of cementation solution is constant, the treatment frequency and interval between injections also affect the final size of the crystals. That is, a longer injection interval produces larger crystals. Because crystal size may affect engineering properties such as strength and permeability, this might be a reason why the engineering properties of the MICP-treated samples varied when the properties of soil treated and $CaCO_3$ content produced are the same.

It has been suggested that large crystals that precipitated at grain contacts that can bond soil particles help to increase the strength of MICP treated-soils (DeJong et al. 2010). In addition, research has recommended that the formation of stable $CaCO_3$ is important for improving the stability of MICP-treated soils (van Paassen 2009). Therefore, based on these results, a long injection interval (23–25 h) might be better compared with a shorter injection interval (3–5 h). This is because when the injection interval is shorter (3–5 h), the crystals are small and coat the surface of the soil

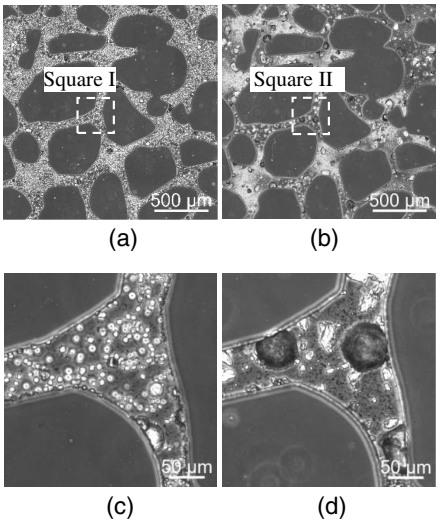

Fig. 14. Microscope images of middle 3 × 3 mm squares of microfluidic chips 1 day after the completion of the 12th cementation solution injection at (a and c) 3–5 h interval; and (b and d) 23–25 h interval. Plots (c) and (d) are magnified images of Square I and Square II in plots (a) and (b), respectively.

particles, whereas when the injection interval is longer (23–25 h), the crystals are larger in size and are more likely to effectively bond the soil particles. Further work is needed to establish a relationship between crystal size and injection intervals based on the findings made in this study, as well as to determine the effect of injection intervals on the engineering properties of MICP-treated samples.

Conclusions

In this study, the MICP process was visualized at the microscale in order to understand the effects of bacterial cells on $CaCO_3$ precipitation, the evolution of the shape and size of the $CaCO_3$ precipitates during the MICP process, and the effect of treatment procedure on the final size of $CaCO_3$ crystals. The main findings of this study are summarized as follows.

Bacterial aggregation was first observed in the glass slide experiments in the mixture of bacterial suspension and cementation solution. Such aggregation was also observed in the staged-injection microfluidic chip experiments after injection of the cementation solution, even though less aggregation was observed than in the glass slide experiment. Bacterial aggregation is an important factor promoting the fixing of bacterial cells in the chip and $CaCO_3$ precipitation where the precipitates grew on top of bacterial aggregates.

Both the glass slide and microfluidic experiments showed that the shape and size of the $CaCO_3$ precipitates change during the MICP process. At first, irregularly shaped $CaCO_3$ precipitates formed during the initial stage of the precipitation process. These precipitates then dissolved as $CaCO_3$ crystals (spherical or rhombohedral) formed. At longer time scales, spherical $CaCO_3$ crystals dissolved at the expense of the growth of rhombohedral $CaCO_3$ crystals. Likewise, small crystals tended to dissolve at the expense of the growth of larger $CaCO_3$ crystals of the same type.

The rhombohedral crystals appeared to be more stable than the spherical crystals, which in turn were more stable than the irregularly shaped precipitates. This is reminiscent of the transformation of irregularly shaped amorphous $CaCO_3$ precipitates to spherical vaterite and then to rhombohedral calcite (Rodriguez-Blanco et al. 2011). Together with the morphological aspects of these structures, one can assume that rhombohedral crystals are calcite, spherical crystals are vaterite, and irregularly shaped precipitates are amorphous $CaCO_3$ precipitates, as suggested by Rodriguez-Blanco et al. (2011) and Chu et al. (2013). Such transformations are common aspects of $CaCO_3$ physical chemistry and must therefore be robust features of MICP in the microfluidic device and in larger-scale applications.

The time-dependent phase transformation of $CaCO_3$ precipitates makes the size of produced MICP crystals highly dependent on the time interval between cementation solution injections during a staged-injection procedure. The average size of $CaCO_3$ crystals was considerably higher when the injection interval was 23–25 h instead of 3–5 h.

This work demonstrates that even though the total amount of $CaCO_3$ might be the same, the size of $CaCO_3$ crystals may be different when different injection intervals are used. This difference would in turn affect the engineering properties of MICP-treated samples, such as permeability, stiffness, and strength. All cementation inside soils decreases permeability, and large crystals at the open pore throat might correspond to the effective $CaCO_3$ required to reduce soil permeability (Al Qabany and Soga 2013). The production of larger crystals at narrow pore throats that are able to bond soil particles might be more efficient in increasing the stiffness and strength of MICP-treated soils (DeJong et al. 2010). Further work involving translation of these findings to real soil applications will be useful for determining a relationship between the treatment process and engineering properties of MICP-treated soils.

The general approach presented here also opens the door to a systematic and quantitative study of other factors likely to affect bacterial aggregation and $CaCO_3$ precipitation process. The size and shape of the pores, as well as the surface properties of the porous medium, can be experimentally controlled to study how soil-specific attributes may influence MICP. Environmental parameters such as temperature would also influence the resulting precipitation dynamics. It is anticipated that in vitro studies of $CaCO_3$ combining microfluidics and imaging will play an important role in optimizing MICP for a broad range of soils and climates.

Acknowledgments

The first author would like to acknowledge Cambridge Commonwealth, European and International Trust, and the China Scholarship Council for financially supporting this research project.

References

Al Qabany, A., and K. Soga. 2013. "Effect of chemical treatment used in MICP on engineering properties of cemented soils." *Géotechnique* 63 (4): 331–339. https://doi.org/10.1680/geot.SIP13.P.022.

Al Qabany, A., K. Soga, and C. Santamarina. 2012. "Factors affecting efficiency of microbially induced calcite precipitation." *J. Geotech. Geoenviron. Eng.* 138 (8): 992–1001. https://doi.org/10.1061/(ASCE)GT.1943-5606.0000666.

Bang, S. S., J. K. Galinat, and V. Ramakrishnan. 2001. "Calcite precipitation induced by polyurethane-immobilized *Bacillus pasteurii*." *Enzyme Microb. Technol.* 28 (4–5): 404–409. https://doi.org/10.1016/S0141-0229(00)00348-3.

Bots, P., L. G. Benning, J.-D. Rodriguez-Blanco, T. Roncal-Herrero, and S. Shaw. 2012. "Mechanistic insights into the crystallization of amorphous calcium carbonate (ACC)." *Cryst. Growth Des.* 12 (7): 3806–3814. https://doi.org/10.1021/cg300676b.

Carteret, C., A. Dandeu, S. Moussaoui, H. Muhr, B. Humbert, and E. Plasari. 2009. "Polymorphism studied by lattice phonon Raman spectroscopy and statistical mixture analysis method. Application to calcium carbonate polymorphs during batch crystallization." *Cryst. Growth Des.* 9 (2): 807–812. https://doi.org/10.1021/cg800368u.

Cheng, L., M. A. Shahin, and D. Mujah. 2017. "Influence of key environmental conditions on microbially induced cementation for soil stabilization." *J. Geotech. Geoenviron. Eng.* 143 (1): 04016083. https://doi.org/10.1061/(ASCE)GT.1943-5606.0001586.

Chu, D. H., M. Vinoba, M. Bhagiyalakshmi, I. Hyun Baek, S. C. Nam, Y. Yoon, and S. K. Jeong. 2013. "CO_{232} system." *RSC Adv.* 3 (44): 21722. https://doi.org/10.1039/c3ra44007a.

Cöelfen, H., and M. Antonietti. 2008. *Mesocrystals and nonclassical crystallization*. New York: Wiley.

DeJong, J. T., M. B. Fritzges, and K. Nüsslein. 2006. "Microbially induced cementation to control sand response to undrained shear." *J. Geotech. Geoenviron. Eng.* 132 (11): 1381–1392. https://doi.org/10.1061/(ASCE)1090-0241(2006)132:11(1381).

DeJong, J. T., B. M. Mortensen, B. C. Martinez, and D. C. Nelson. 2010. "Bio-mediated soil improvement." *Ecol. Eng.* 36 (2): 197–210. https://doi.org/10.1016/j.ecoleng.2008.12.029.

Dhami, N. K., M. S. Reddy, and A. Mukherjee. 2013. "Biomineralization of calcium carbonates and their engineered applications: A review." *Front. Microbiol.* 4: 314. https://doi.org/10.3389/fmicb.2013.00314.

El Mountassir, G., R. J. Lunn, H. Moir, and E. MacLachlan. 2014. "Hydrodynamic coupling in microbially mediated fracture mineralization: Formation of self-organized groundwater flow channels." *Water Resour. Res.* 50 (1): 1–16. https://doi.org/10.1002/2013WR013578.

Ganendra, G., W. De Muynck, A. Ho, E. C. Arvaniti, B. Hosseinkhani, J. A. Ramos, and N. Boon. 2014. "Formate oxidation-driven calcium carbonate precipitation by *Methylocystis parvus* OBBP." *Appl. Environ. Microbiol.* 80 (15): 4659–4667. https://doi.org/10.1128/AEM.01349-14.

Hammes, F., and W. Verstraete. 2002. "Key roles of pH and calcium metabolism in microbial carbonate precipitation." *Rev. Environ. Sci. Biotechnol.* 1 (1): 3–7. https://doi.org/10.1023/A:1015135629155.

Jiang, N.-J., K. Soga, and M. Kuo. 2017. "Microbially induced carbonate precipitation for seepage-induced internal erosion control in sand-clay mixtures." *J. Geotech. Geoenviron. Eng.* 143 (3): 04016100. https://doi.org/10.1061/(ASCE)GT.1943-5606.0001559.

Kawano, J., N. Shimobayashi, M. Kitamura, K. Shinoda, and N. Aikawa. 2002. "Formation process of calcium carbonate from highly supersaturated solution." *J. Cryst. Growth* 237 (1–4): 419–423. https://doi.org/10.1016/S0022-0248(01)01866-8.

Keykha, H. A., M. Zareian, B. B. K. Huat, A. Asadi, and S. Kawasaki. 2015. "Electrokinetic properties of pasteurii and aquimarina bacteria." *Environ. Geotech.* 2 (3): 181–188. https://doi.org/10.1680/envgeo.13.00072.

Lian, B., Q. Hu, J. Chen, J. Ji, and H. H. Teng. 2006. "Carbonate biomineralization induced by soil bacterium *Bacillus megaterium*." *Geochim. Cosmochim. Acta* 70 (22): 5522–5535. https://doi.org/10.1016/j.gca.2006.08.044.

Lin, H., M. T. Suleiman, D. G. Brown, and E. Kavazanjian. 2016. "Mechanical behavior of sands treated by microbially induced carbonate precipitation." *J. Geotech. Geoenviron. Eng.* 142 (2): 04015066. https://doi.org/10.1061/(ASCE)GT.1943-5606.0001383.

Martinez, B. C., J. T. DeJong, T. R. Ginn, B. M. Montoya, T. H. Barkouki, C. Hunt, B. Tanyu, and D. Major. 2013. "Experimental optimization of microbial-induced carbonate precipitation for soil improvement." *J. Geotech. Geoenviron. Eng.* 139 (4): 587–598. https://doi.org/10.1061/(ASCE)GT.1943-5606.0000787.

Mitchell, A. C., and F. G. Ferris. 2006. "The influence of *Bacillus pasteurii* on the nucleation and growth of calcium carbonate." *Geomicrobiol. J.* 23 (3–4): 213–226. https://doi.org/10.1080/01490450600724233.

Montoya, B. M., J. T. DeJong, and R. W. Boulanger. 2013. "Dynamic response of liquefiable sand improved by microbial-induced calcite precipitation." *Géotechnique* 63 (4): 302–312. https://doi.org/10.1680/geot.SIP13.P.019.

Morse, J. W., R. S. Arvidson, and A. Lüttge. 2007. "Calcium carbonate formation and dissolution." *Chem. Rev.* 107 (2): 342–381. https://doi.org/10.1021/cr050358j.

Ogino, T., T. Suzuki, and K. Sawada. 1987. "The formation and transformation mechanism of calcium carbonate in water." *Geochim. Cosmochim. Acta* 51 (10): 2757–2767. https://doi.org/10.1016/0016-7037(87)90155-4.

Phillips, A. J., E. Lauchnor, J. Eldring, R. Esposito, A. C. Mitchell, R. Gerlach, and L. H. Spangler. 2013. "Potential CO_2 leakage reduction through biofilm-induced calcium carbonate precipitation." *Environ. Sci. Technol.* 47 (1): 142–149. https://doi.org/10.1021/es301294q.

Rodriguez-Blanco, J. D., S. Shaw, and L. G. Benning. 2011. "The kinetics and mechanisms of amorphous calcium carbonate (ACC) crystallization to calcite, via vaterite." *Nanoscale* 3 (1): 265–271. https://doi.org/10.1039/C0NR00589D.

Stocks-Fischer, S., J. K. Galinat, and S. S. Bang. 1999. "Microbiological precipitation of $CaCO_3$." *Soil Biol. Biochem.* 31 (11): 1563–1571. https://doi.org/10.1016/S0038-0717(99)00082-6.

van Paassen, L. 2009. "Biogrout: Ground improvement by microbially induced carbonate precipitation." Ph.D. thesis, Dept. of Civil Engineering and Geosciences, Delft Univ. of Technology.

van Paassen, L. A., R. Ghose, T. J. M. van der Linden, W. R. L. van der Star, and M. C. M. van Loosdrecht. 2010. "Quantifying biomediated ground improvement by ureolysis: Large-scale biogrout experiment." *J. Geotech. Geoenviron. Eng.* 136 (12): 1721–1728. https://doi.org/10.1061/(ASCE)GT.1943-5606.0000382.

Wang, Y., K. Soga, J. T. DeJong, and A. J. Kabla. 2018. "A microfluidic chip and its use in characterizing the particle-scale behavior of microbial-induced carbonate precipitation (MICP)." *Géotechnique* 1–9. https://doi.org/10.1680/jgeot.18.P.031.

Wang, Y., K. Soga, and N.-J. Jiang. 2017. "Microbial induced carbonate precipitation (MICP): The case for microscale perspective." In *Proc., 19th Int. Conf. on Soil Mechanics and Geotechnical Engineering*, edited by W. Lee, J.-S. Lee, H.-K Kim, and D.-S. Kim, 1099–1102. Seoul.

Wei, H., Q. Shen, Y. Zhao, D. J. Wang, and D. F. Xu. 2003. "Influence of polyvinylpyrrolidone on the precipitation of calcium carbonate and on the transformation of vaterite to calcite." *J. Cryst. Growth* 250 (3–4): 516–524. https://doi.org/10.1016/S0022-0248(02)02484-3.

Whiffin, V. S., L. A. van Paassen, and M. P. Harkes. 2007. "Microbial carbonate precipitation as a soil improvement technique." *Geomicrobiol. J.* 24 (5): 417–423. https://doi.org/10.1080/01490450701436505.

Yoon, J. H., K. C. Lee, N. Weiss, Y. H. Kho, K. H. Kang, and Y. H. Park. 2001. "*Sporosarcina aquimarina* sp. nov., a bacterium isolated from seawater in Korea, and transfer of *Bacillus globisporus* (Larkin and Stokes 1967), *Bacillus psychrophilus* (Nakamura 1984) and *Bacillus pasteurii* (Chester 1898) to the genus *Sporosarcina* as Sporosa." *Int. J. Syst. Evol. Microbiol.* 51 (3): 1079–1086. https://doi.org/10.1099/00207713-51-3-1079.

Zhou, G. T., J. C. Yu, X. C. Wang, and L. Z. Zhang. 2004. "Sonochemical synthesis of aragonite-type calcium carbonate with different morphologies." *New J. Chem.* 28 (8): 1027–1031. https://doi.org/10.1039/b315198k.